Direct inference of the distribution of fitness effects of spontaneous mutations from recombinant inbred *C. elegans* mutation accumulation lines

Timothy A. Crombie[1,2,6], Moein Rajaei[1,], Ayush S. Saxena[1], Lindsay M. Johnson[1,3], Sayran Saber[1,7], Robyn E. Tanny[2,4], José Miguel Ponciano[1], Erik C. Andersen[2,4*], Juannan Zhou[1,*], and Charles F. Baer [1,5,*]

[1]*Department of Biology, University of Florida, Gainesville, FL, 32611, USA*

[2] *Department of Molecular Biosciences, Northwestern University, Evanston, IL 60208, USA*

[3] *Present address: Avenge Bio, Inc., Natick, MA, USA*

[4] *Department of Biology, Johns Hopkins University, Baltimore, MD 21218, USA*

[5] *University of Florida Genetics Institute, Gainesville, FL, 32611, USA*

[6] *Present address: Florida Institute of Technology, Melbourne FL*

[7] *Present address: Florida International University, Miami, FL*

[*]Corresponding authors: erik.andersen@jhu.edu; juannanzhou@ufl.edu, cbaer@ufl.edu

Abstract

The distribution of fitness effects (DFE) of new mutations plays a central role in evolutionary biology. Estimates of the DFE from experimental Mutation Accumulation (MA) lines are compromised by the complete linkage disequilibrium (LD) between mutations in different lines. To reduce LD, we constructed two sets of recombinant inbred lines from a cross of two *C. elegans* MA lines. One set of lines ("RIAILs") was intercrossed for ten generations prior to ten generations of selfing; the second set of lines ("RILs") omitted the intercrossing. Residual LD in the RIAILs is much less than in the RILs, which affects the inferred DFE when the sets of lines are analyzed separately. The best-fit model estimated from all lines (RIAILs + RILs) infers a large fraction of mutations with positive effects (~40%); models that constrain mutations to have negative effects fit much worse. The conclusion is the same using only the RILs. For the RIAILs, however, models that constrain mutations to have negative effects fit nearly as well as models that allow positive effects. When mutations in high LD are pooled into haplotypes, the inferred DFE becomes increasingly negative-skewed and leptokurtic. We conclude that the conventional wisdom - most mutations have effects near zero, a handful of mutations have effects that are substantially negative and mutations with positive effects are very rare – is likely correct, and that unless it can be shown otherwise, estimates of the DFE that infer a substantial fraction of mutations with positive effects are likely confounded by LD.

INTRODUCTION

The distribution of fitness effects (DFE) of new mutations is of fundamental importance in numerous areas of evolutionary biology (FISHER 1930; ORR 2000; PECK *et al.* 1997; SCHULTZ and LYNCH 1997; ZHANG *et al.* 2004), as well as having practical applications, including human genetic disease (AGARWAL *et al.* 2023; BOYLE *et al.* 2017; EYRE-WALKER 2010; MORROW and CONNALLON 2013) and cancer (CANNATARO *et al.* 2016; CANNATARO and TOWNSEND 2018; DURRETT *et al.* 2010). The DFE can be estimated from data in two ways: indirectly from patterns of sequence variation within and between species (BOYKO *et al.* 2008; GILBERT *et al.* 2021; JAMES *et al.* 2023; JOHRI *et al.* 2020; KEIGHTLEY and EYRE-WALKER 2010; KIM *et al.* 2017; KOUSATHANAS and KEIGHTLEY 2013; LOEWE and CHARLESWORTH 2006; TATARU *et al.* 2017), or directly from comparisons between genotypes differing by a known (or estimated) set of mutations (BÖNDEL *et al.* 2019; DAVIES *et al.* 1999; KEIGHTLEY 1994; RAMANI *et al.* 2012; SHEN *et al.* 2022; THATCHER *et al.* 1998). Each method has strengths and limitations. Estimation from the standing variation incorporates a vastly larger number of mutations than could ever be assessed experimentally, the effects of very weak selection are detectable (at least in aggregate), and effects are integrated over the entire spectrum of environmental and genomic contexts experienced by the organism in question. However, the method has several important limitations. First, the effects of selection must be jointly estimated with the effects of demography, which are necessarily greatly simplified for analytical tractability (JOHRI *et al.* 2020; KEIGHTLEY and EYRE-WALKER 2007; LI *et al.* 2012). Second, there is little information about the tail of the distribution for which selection is strong on an evolutionary timescale but weak over the course of a few generations ($s \approx 1\%$) (KOUSATHANAS and KEIGHTLEY 2013). Third, the method assumes there is a class of mutations that are selectively neutral to serve as a

58 reference; the extent to which that assumption is met is an empirical issue requiring independent
59 validation (KRUGLYAK *et al.* 2023; SHEN *et al.* 2022). Finally, there is no way to connect the
60 DFE back to phenotypic traits.

61 Direct estimation from fitness differences between known genotypes has the advantage of
62 being conceptually unambiguous - if two groups differ by a single mutation and differ in fitness
63 by some amount y, the effect of the mutation is y. Constructing two populations that differ by
64 one or a few mutations is straightforward: known mutations can be introgressed or otherwise
65 engineered (e.g., by CRISPR) into a common genetic background to provide "nearly isogenic
66 lines" (NILs). Recent advances in CRISPR technology have made it possible to engineer large
67 panels of NILs in yeast and other microbes (SHARON *et al.* 2018; SHEN *et al.* 2022). However,
68 constructing enough NILs to provide a meaningful estimate of the DFE remains a daunting
69 proposition in multicellular organisms. Single-gene "knockout panels", in which genes are
70 systematically inactivated and the fitness effects documented, have been tremendously important
71 in informing our understanding of the functional aspects of the genome (e.g., KIM *et al.* 2010;
72 RAMANI *et al.* 2012; THATCHER *et al.* 1998), but knockout mutations constitute only a small part
73 of the mutational spectrum and do not provide an unbiased estimate of the DFE.

74 Mutation accumulation (MA) experiments, in which spontaneous mutations are allowed
75 to accumulate in the (near) absence of natural selection, provide the opportunity to estimate the
76 DFE of a (nearly) unbiased set of mutations (HALLIGAN and KEIGHTLEY 2009; KATJU and
77 BERGTHORSSON 2019). However, within an MA line, all mutations are in complete linkage
78 disequilibrium, which renders individual mutational effects inestimable.

79 Here we employ a classical line-cross strategy with MA lines, to break down the linkage
80 disequilibrium among the accumulated mutations. We then combine whole-genome sequencing

with high-throughput competitive fitness assays to estimate the DFE of a set of 169 spontaneous mutations. This strategy was first employed by BÖNDEL *et al.* (2019) with the unicellular green alga *Chlamydomonas reinhardtii*. We crossed two parental *C. elegans* mutation accumulation (MA) lines derived from the same genetically homogeneous ancestor to get F1 hybrids that are segregating at all mutant loci. The F1s were reciprocally crossed, and from the F2s we constructed two sets of recombinant inbred lines (**Supplemental Figure 1**). For the first set, F2s were further crossed prior to inbreeding to construct a set of Recombinant Inbred Advanced Intercross Lines (RIAILs). For the second set, we omitted the intercrossing step and proceeded directly to the inbreeding step; these lines are classical RILs. We refer to the full set of lines as RI(AI)Ls for brevity. RI(AI)Ls were assayed for competitive fitness against a marked competitor strain nearly isogenic for the ancestral genome, and multilocus genotypes inferred by whole-genome sequencing at low (2-3X) coverage. The strategy is conceptually analogous to QTL analysis, except the variant loci are not simply markers, but rather are the QTL themselves.

METHODS

1. Experimental Methods

1.1 Mutation Accumulation (MA) lines.

The details of the MA experiment have been reported elsewhere (BAER *et al.* 2005). Briefly, 100 replicate lines were initiated from a single, highly inbred N2 strain hermaphrodite, and propagated under standard laboratory conditions for a maximum of 250 generations by transfer of a single immature hermaphrodite at four-day intervals. Under this protocol the effective population size, $N_e \approx 1$, and all but the most highly deleterious mutations are effectively neutral.

103 The progenitor (G0) was cryopreserved at the outset of the experiment, and surviving MA lines
104 were cryopreserved upon culmination of the MA phase.

105 *1.2 Recombinant Inbred (Advanced Intercross) Lines*.

106 Two MA lines (MA530 and MA563) were chosen as parents for a set of recombinant inbred
107 advance intercross lines (RIAILs) or simple recombinant inbred lines (RILs). The parental lines
108 were chosen on the basis of their near-average decline in lifetime reproductive success (~20%)
109 over four assays after 200 and 220 generations of MA at two different assay temperatures (20°
110 and 25° (BAER *et al.* 2006). The original plan was to construct a set of 600 RIAILs, with ten
111 generations of intercrossing followed by ten generations of selfing, using the "random pair
112 mating with equal contributions of each parent" design of ROCKMAN and KRUGLYAK (2008; see
113 their Figure 1). However, many crosses failed during the intercrossing phase, so we abandoned
114 the intercrossing and completed the set of lines with RILs. The final set of 517 genotyped lines
115 includes 192 RIAILs and 325 RILs. Details of the crossing schemes are given in **Section I of**
116 **the Supplemental Material**.

117 *1.3 Competitive fitness assays*.

118 To assay competitive fitness, an L1-stage focal strain worm and an L1 GFP-marked competitor
119 (strain VP604) were placed together on a plate seeded with bacterial food and allowed to
120 reproduce. Upon exhaustion of the bacterial food, worms were washed from the plate and
121 counted using a Union Biometrica BioSorter™. The natural logarithm of the ratio of the
122 frequencies of the two types, $W=\log[(p/1-p)]$, is proportional to the difference in fitness between
123 the focal strain (frequency = p) and the competitor strain (frequency = $1-p$) (LATTER and SVED
124 1994). The assay is described in detail in Appendix 1 of YEH *et al.* (2018) and summarized in
125 **Section II of the Supplemental Material**.

126 *1.4 Genome sequencing, variant calling, and genotyping.*

127 RI(AI)L genomes were sequenced at low (~2-3X) coverage with 150-bp paired-end Illumina
128 sequencing, using standard methods. Details of sequencing and variant calling are given in
129 **Section III of the Supplemental Material**. Raw sequence data (fastq) of the RI(AI)Ls have
130 been deposited in the NCBI SRA under project number PRJNA1083210. Genome sequences for
131 the G0 progenitor and the parent MA lines have been previously reported (RAJAEI *et al.* 2021;
132 SAXENA *et al.* 2019).

133 *1.5. Imputation*. Given the low (2-3X) sequencing coverage, approximately 1/3 of the data
134 (35.2%) are missing, i.e., the genotype at a given locus was not called as either homozygote.
135 The mean number of loci successfully genotyped per RI(AI)L is 109, and the mean number of
136 RI(AI)Ls for which a locus was scored is 335. To account for the missing genotype information,
137 we constructed a computational procedure to impute the missing data by leveraging linkage
138 disequilibrium (LD; see next section) between segregating sites. Specifically, we used the
139 masked language modeling approach from natural language processing to build a predictive
140 model for the missing alleles. The imputation model is built on the transformer architecture,
141 which has been widely used for modeling natural languages as well as biological sequences such
142 as DNAs and proteins (JI *et al.* 2021; RIVES *et al.* 2021). The model output consists of the
143 predicted log-probability for all possible states per site, i.e., the MA530 or MA563 allele. The
144 details of the model are given in **Section IV of the Supplemental Material**.

145 To assess the model's performance, we performed 100 rounds of validation. For each
146 round, all RI(AI)L genotypes were used for training, but with one percent of the called alleles
147 randomly masked. Across the 100 rounds, we observed a high imputation accuracy on the
148 masked positions: mean ± 1 SD prediction accuracy = 90.3 ± 1.5%. Cases in which the imputed

149 allele differs from the called allele include errors in the initial call, so 90% is a conservative
150 estimate of the true prediction accuracy. The final imputed genotypes (**Supplemental Table 1**)
151 were generated by retraining the model on all RI(AI)L genotypes using all available allele
152 information.

153 *1.6. Linkage Disequilibrium (LD)*

154 Alleles from the two parents, MA530 and MA563, are initially in complete coupling (positive)
155 linkage disequilibrium in the F1. However, mutant alleles occur in both parental genomes, so
156 although the initial LD between pairs of mutant alleles is complete, the sign of the association
157 (positive or negative) depends on which parental genomes the mutations occurred. Measures of
158 LD that do not account for the sign of the association are agnostic with respect to whether alleles
159 are coded by the parent of origin or as ancestral (0) vs. mutant (1); the value is the same either
160 way. Measures of LD that do account for the sign of the association may differ by sign
161 depending on if the alleles are coded by parent of origin vs. ancestral vs. mutant. For our
162 purposes, it is more meaningful to code alleles as ancestral or mutant.

163 The pairwise coefficient of linkage disequilibrium, $D=p_{A1B1}-p_{A1}p_{B1}$ where p_{A1B1} is the
164 frequency of the double-mutant (*A1B1*) haplotype at the A and B loci, p_{A1} is the frequency of the
165 mutant allele at the A locus and p_{B1} is the frequency of the mutant allele at the B locus. The
166 expected allele frequency in the RI(AI)Ls is 0.5 at all segregating loci, but the observed
167 frequencies will vary due to sampling. We report two measures of LD, the squared coefficient of
168 correlation, r^2, and $D^*=D/|Dmax|$, where $|Dmax|= \min[p_{A1}(1-p_{B1})], (1-p_{A1})p_{B1}]$; r^2 is constrained
169 non-negative and D^* can take on values [-1,1]. Note that our D^* is the familiar D' but with the
170 sign retained. We calculated r^2 and D^* among all pairs of the 169 loci using the PLINK v1.9
171 commands '--r2' and '--r dprime-signed' respectively (PURCELL *et al.* 2007). We also report the

172 mean pairwise intra-chromosomal and inter-chromosomal LD for (1) all lines (n = 517), (2) RILs
173 only (n = 325), and (3) RIAILs only (n = 192). To visualize intra-chromosomal pairwise LD we
174 used the ggplot2 package v3.4.4 for R Statistical Software v4.2.3 (WICKHAM 2009).
175 *1.7. Heritability*. We estimated the broad-sense heritability (H^2) of W from the among-line (i.e.,
176 among-RI(AI)L) component of variance estimated from the general linear model (GLM) $y_{ijk} = \mu$
177 $+ \alpha_i + \beta_{ij} + \varepsilon_{ijk}$, where y_{ijk} is the value of W, μ is the overall mean, α_i is the random effect of
178 Block i, β_{ij} is the random effect of Line j in Block i, and ε_{ijk} is the residual effect of Replicate k of
179 Line j in Block i. Because the RI(AI)Ls are homozygous lines derived from a cross of
180 homozygous parents, $V_G = V_L$, where V_L is the among-line component of variance (FALCONER
181 1989, Ch. 15) and the broad-sense heritability $H^2=V_G/V_P$, where V_P is the total phenotypic
182 variance. Variance components were estimated by restricted maximum likelihood (REML), as
183 implemented in the MIXED procedure of SAS v. 9.4. Variance components were first estimated
184 hierarchically (i.e., the within-line and among-line components of variance were estimated
185 separately for each block), and tested against models with the variance pooled over blocks. The
186 best model was ascertained by the Bayesian Information Criterion. Statistical significance of the
187 among-line variance was assessed by likelihood-ratio test (LRT), wherein the model with the line
188 term included was tested against the simpler model with Line excluded. The models are nested,
189 so twice the difference in log(likelihood) is asymptotically Chi-square distributed with degrees of
190 freedom equal to the difference in the number of parameters estimated.
191 To account for the possibility that some of the among-line variance was due to factors
192 other than genotype, we included a set of six "pseudolines" of the G0 ancestor and of each
193 parental MA line in each assay block, which are the experimental equivalent of RILs except they

194 are genetically homogeneous, and any among-(pseudo)line variance must be due to causes other
195 than variation among genes. Pseudolines were analyzed identically to the RI(AI)Ls.
196 We next estimated the proportion of the total broad-sense heritability not explained by
197 the cumulative additive effects of the mutations, H^2*, from the full (imputed) dataset, as follows.
198 First, we calculated the multiple regression $y_{ijk} = \mu + \boldsymbol{\beta}\mathbf{x} + \varepsilon$, where y_{ijk} is the value of W as
199 before, μ is the overall mean, **x** is the vector of genotypes at mutant loci 1-169, $\boldsymbol{\beta}$ is the vector of
200 regression coefficients, and ε is the residual effect. We then re-estimated the linear model from
201 above, $y^*_{ijk} = \mu + \alpha_i + \beta_{ij} + \varepsilon_{ijk}$, where the terms are as before, where the y^*_{ijk} are the residuals of
202 the multiple regression of W on the multilocus genotype, **x**. The difference H^2- H^2* is the
203 narrow-sense heritability h^2, i.e., the fraction of the total phenotypic variance explained by the
204 additive effects of the mutations. Statistical significance of h^2 was assessed by randomly
205 permuting estimates of W among replicates and re-calculating h^2.
206
207 *2. Estimation of the DFE*
208 *2.1. Marginal effects*. The simplest way to measure the phenotypic effect of a mutation at locus *i*
209 is from the average difference in the trait between lines that have the mutant allele and lines that
210 have the ancestral allele at locus *i*. We refer to the mutational effects calculated in this way as
211 the marginal effects. Confidence intervals and approximate standard errors of marginal effects
212 were calculated from 1000 bootstrap replicates, holding the number of lines in each category
213 (mutant, wild-type) constant in each (re)sample.
214 *2.2. Bayesian MCMC*. We take a fully Bayesian approach to estimate the posterior distribution
215 of all genetic and non-genetic parameters. The basic model is the same as in section 1.7 above,
216 such that the observed fitness of replicate *k* of line *j* in block *i* is: $y_{ijk} = \mu + \alpha_i + \boldsymbol{\beta}^T\mathbf{x_j} + \varepsilon_{ijk.}$ The

217 vector $\boldsymbol{\beta}$ contains the effects for the 169 mutations. We fit a series of models with increasing
218 complexity in the prior distribution of $\boldsymbol{\beta}$, to test different hypotheses regarding the DFE of the
219 mutations. In all models, the grand mean, μ, follows an uninformative normal distribution with
220 mean zero and SD = 10. The individual block effects follow normal distributions with mean 0
221 and SD = 1, given the small variation in block effects when averaged over lines (SD = 0.13). The
222 models tested are summarized in **Table 1**.

223 To begin, in model 1 ("neutral model") mutational effects are constrained to 0, i.e., $\boldsymbol{\beta} = 0$.
224 In model 2 ("uniform effect model"), all mutations in the vector $\boldsymbol{\beta}$ have a constant effect (u),
225 such that $y_{ijk} = \mu + \alpha_i + m_j \times u + \varepsilon_{ijk.}$, where m_j is the number of mutant alleles in line j.
226 Model 3 ("neutral + uniform effect model") assumes that mutations in vector $\boldsymbol{\beta}$ follow identical
227 independent distributions such that the m-th mutation, β_m, has a probability $1 - q$ of being
228 neutral, and q of having a nonzero constant effect u, such that $\beta_m = w \times u$, where w is sampled
229 from a Bernoulli distribution with parameter q, which in turn is drawn from an uninformative
230 Beta prior with shape parameters = 2. In both the uniform effect model and the neutral +
231 uniform effect model, the constant mutational effect u follows a normal prior with mean 0 and
232 SD = 10. Model 4 (neutral + uniform positive effect + uniform negative effect, "3-effect
233 model") in addition assumes that mutations can take both constant positive or negative effects,
234 such that $\beta_m = w \times (z \times u^+ - (1 - z) \times u^-)$. Similarly, w is a Bernoulli random variable with the
235 probability q, equal to the probability that a mutation is non-neutral, which follows the same
236 distribution as model 3. The parameter z controls the conditional probability of a nonneutral
237 mutation having the positive effect, and is a Bernoulli random variable with probability p^+,
238 which follows an uninformative Beta distribution with shape parameters = 2. The constant

239 positive/negative effects u_{pos}/u_{neg} follow an uninformative normal distribution with mean 0 and
240 SD = 10.

241 In addition to these constant-effects models, we tested three models in which mutational
242 effects are sampled from a continuous Gamma distribution. In model 5 ("negative gamma"), all
243 mutations are assumed to have negative (i.e., deleterious) effects, with effect sizes sampled
244 identically and independently from a Gamma distribution, whose shape and rate parameters
245 follow uninformative half normal distributions (SD = 10). In model 6 ("symmetric gamma") and
246 model 7 ("asymmetric gamma"), mutations can have either positive or negative effects, such that
247 we can express individual mutation effects as $\beta_m = z \times \beta_m^+ - (1 - z) \times \beta_m^-$. Similar to model 4, z
248 is a Bernoulli random variable with probability p^+, which follows a symmetric Beta distribution.
249 The positive (negative) effect sizes, β_m^+ (β_m^-) are in turn sampled from their respective Gamma
250 distributions, as in Model 5. The only difference between model 6 and 7 is that in model 6, β_m^+
251 and β_m^- follow the same Gamma distribution, whereas in model 7, the Gamma distributions for
252 the positive and negative effect sizes are allowed to be different.

253 Bayesian inference for all models was implemented in the statistical software PyMC3
254 v5.10 (SALVATIER *et al.* 2016). The No-U-Turn-Sampler was employed to acquire posterior
255 samples. Continuous random variables were sampled using the Hamiltonian Monte Carlo
256 method which relies on gradients calculated using automatic differentiation, whereas discrete
257 random variable were sampled using the Metropolis algorithm. To account for the uncertainty in
258 the genotypes due to missing alleles, for each model we performed 50 independent Monte Carlo
259 runs, each with missing alleles sampled from independent Bernoulli distributions with
260 probability predicted by the trained imputation model. For each model and genotype replicate,
261 we ran 4 parallel Monte Carlo chains, each with 1000 warm up steps and 4000 sampling steps.

262 We used the R-hat statistic (VEHTARI *et al.* 2021) as a diagnostic of model divergence, which
263 compares the parameter estimates between and within chains. R-hat is greater than 1 if the chains
264 are not well mixed, such that the between and within-chain sample distributions disagree.
265 We used a Bayesian model selection procedure to identify the best model. Specifically,
266 for each model we estimated the leave-one-out expected log pointwise predictive density (ELPD
267 LOO) model fit, equal to the mean expected log likelihood of the observed fitness of a random
268 individual given its genotype, calculated based on a model fitted using the full data set minus the
269 focal individual. The procedure is implemented in PyMC3 based on the approximate method
270 introduced by VEHTARI *et al.* (2017) The ELPD LOO scores for all 50 genotype replicates were
271 averaged to provide an overall goodness-of-fit score for each model.
272
273 **RESULTS:**
274 *Linkage Disequilibrium*
275 The purpose of constructing RI(AI)Ls is to break up the linkage disequilibrium between
276 mutations, to permit estimation of the effects of individual mutations. That effort was only
277 partially, and variably, successful. Averaged over all lines (RILs + RIAILs), intrachromosomal
278 LD as measured by median r^2 is 0.12 (**Figure 1; Supplemental Figure 2**). However, LD is
279 much higher in the RILs (median $r^2 = 0.28$) than in the RIAILs (median $r^2 = 0.045$). Ten
280 generations of advanced intercrossing was effective in breaking up LD, on average, but regions
281 of near-complete LD remain even in the RIAILs. Inspection of **Figure 1** reveals that regions of
282 high LD are concentrated in the chromosome centers, as expected given the reduced rate of
283 crossing over in centers relative to arms, although there are also regions of high LD in
284 chromosome arms where mutations are tightly clustered. Interchromosomal LD is near 0 in both

285 RILs and RIAILs (**Supplemental Figure 3**), indicating a trivial role for sampling variance in

286 maintaining LD.

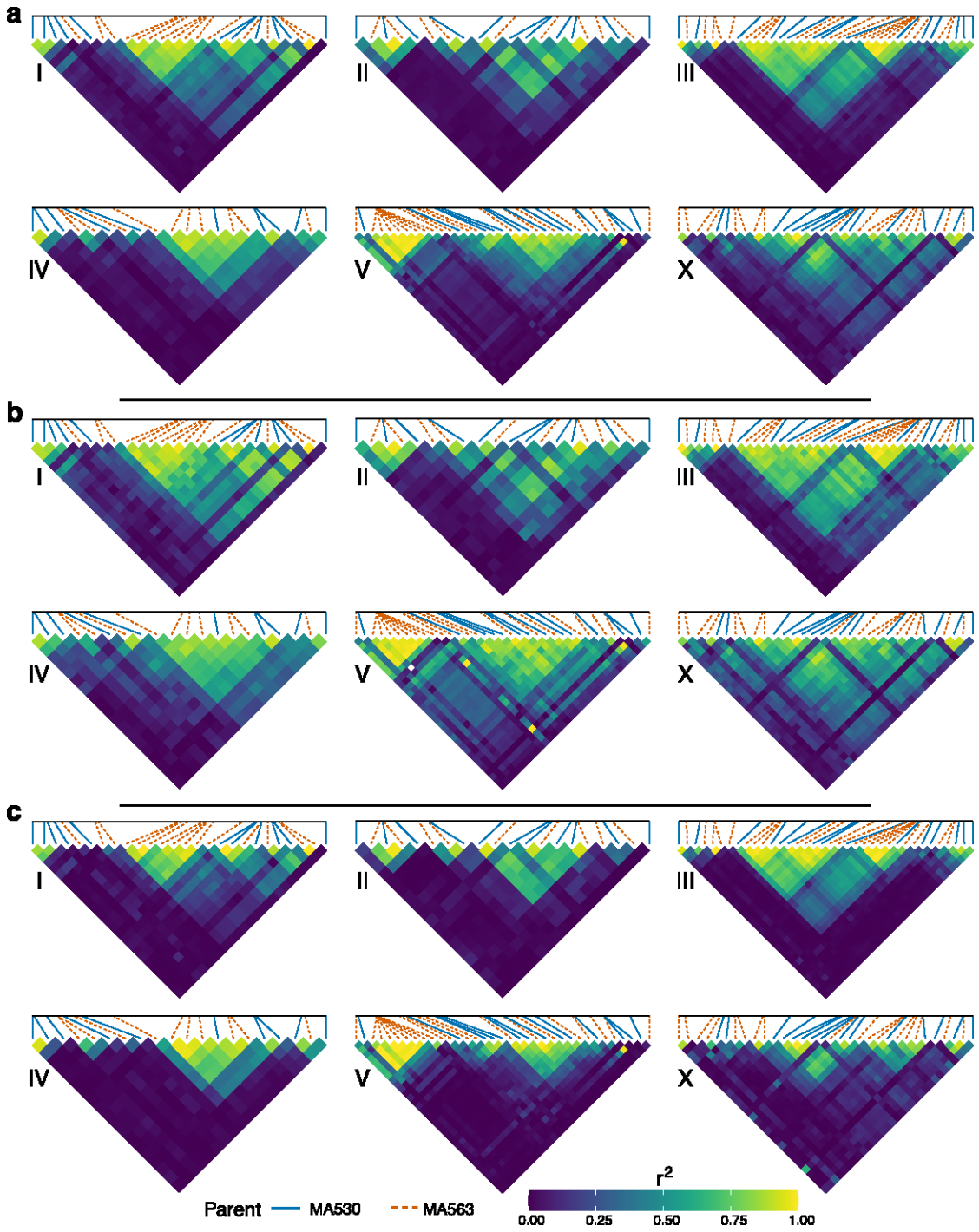

287

288 **Figure 1 - Intrachromosomal pairwise linkage disequilibrium (LD).** (**a**) Pairwise LD (r^2)
289 calculated with all lines (RIAILs + RILs), (**b**) RILs only, and (**c**) RIAILs only. Each heat map
290 represents a chromosome with pairwise LD (r^2) between mutant loci colored as shown in the

legend. The colored lines above each chromosome represent the parental origin of the mutant allele (MA530-solid blue, MA563-dashed orange). These lines also show the relative physical position of mutant loci across each chromosome; the far-left vertical line represents the first mutant locus on the chromosome and the far-right vertical line represents the last mutant locus.

Heritability

Our goal is to estimate the effects of spontaneous mutations on fitness. To begin, we ask: is there heritable variation in competitive fitness among the RI(AI)Ls? The broad-sense heritability of *W* including all RI(AI)Ls, H^2=0.30 (bootstrap SEM=0.023; LRT p<0.0001). Estimates of H^2 were similar for RIAILs (H^2=0.325 $\pm$ 0.036, LRT p<0.0001) and RILs (H^2=0.278$\pm$ 0.029, LRT p<0.0001). Including all RI(AI)Ls, narrow-sense heritability, estimated from the residuals of the multiple regression of *W* on multilocus genotype, h^2 = 0.16 (permutation test, P<0.001; averaged over 1000 permutations of the data, random h^2 = 0.023, max=0.048). The cumulative additive effects of the 169 segregating spontaneous mutations explain approximately half of the total heritable variance in *W*. By way of comparison, H^2 for competitive fitness from a set of 28 *C. elegans* wild isolates was 0.49, although the assays in the two studies are not directly comparable (TEOTÓNIO *et al.* 2006).

Considering RIAILs and RILs separately, h^2 of the RILs is similar to the estimate from the full dataset (h^2 = 0.20, n=325). The same analysis for RIAILs gives a REML point estimate of V_L=0 (i.e., there is no among-line variance of the residuals), which taken at face value implies that additive effects of the multilocus genotype completely explain H^2. A more conservative interpretation is that the smaller number of RIAILs (n=192) provides insufficient power to estimate a relatively small among-line component of variance once the additive effects are accounted for.

315 Variation among lines may have non-genetic causes. To account for that possibility, we
316 estimated variance components among sets of "pseudolines" of the G0 ancestor of the parental
317 lines, and of the MA530 and MA563 parental lines. These controls are not powerful (n=30
318 pseudolines, 6 per block), but in all three cases the REML estimate of the among-pseudoline
319 component of variance, $V_L = 0$. Thus, we infer the remaining unexplained broad-sense
320 heritability is due to some combination of epistasis, transgenerational epigenetic inheritance
321 (TEI), and/or residual (but small) genotype-environment correlations.

322 *Relationship between number of mutations and mean fitness*

323 If all mutational effects are equal and in the same direction (i.e., the Bateman-Mukai criteria
324 (MUKAI 1964)), the slope of the regression of *W* on the number of mutant alleles carried by a line
325 will equal the average effect of a mutation. Averaged over all RI(AI)Ls, accounting for variation
326 among assay blocks and removing two outlying lines, the regression of *W* on number of
327 mutations is not significantly different from 0 (slope = -0.0051, $F_{1,509}=1.83$, $P>0.17$), although
328 the trend suggests that mutations are deleterious, on average.

329 *Relationship between mutational effect and mutant allele frequency*

330 The expected frequency of segregating neutral alleles in the RI(AI)Ls is 0.5. Selection was
331 minimally effective in the crossing and inbreeding phases ($N_e \approx 2$), but it was not absent. If most
332 mutations are deleterious and if deleterious alleles were preferentially removed by selection, then
333 (*i*) the average frequency of mutant alleles will be < 0.5, and (*ii*), there should be a negative
334 relationship between allele frequency and mutational effect size. The mean observed mutant
335 allele frequency is 0.500 (range = 0.287-0.675). The correlation between mutant allele
336 frequency p_i at the *i*th locus and the marginal effect u_i, $r_{pu}= 0.15$ (**Supplemental Figure 4**).

Thus, we infer that selection did not systematically skew mutant allele frequencies away from the expected neutral frequency.

The Bayesian posterior DFE.

To infer the DFE, we tested a series of seven increasingly complex models, using the Bayesian MCMC analysis outlined in the Methods. Because of the discrepancy in average LD between the RIAILs and the RILs, all analyses were first done on the full set of RI(AI)Ls, and repeated on RIAILs and RILs separately.

As a first step, we tested for model convergence, using the R-hat statistic. We observed no divergence between the four parallel Markov chains, indicated by R-hat < 1 in all cases (VEHTARI *et al.* 2021). Model performance, as measured by the Bayesian leave-one-out expected log pointwise predictive density (LOO-ELPD, VEHTARI *et al.* 2021) averaged across 50 genotype replicates, is summarized in **Table 1**. Posterior means and 95% credible intervals of model parameters are given in **Supplemental Table 2**.

Table 1. Comparison of seven competing Bayesian models fitted to the genotype and phenotype data of all RILs and RIAILs, and separately to RILs and RIAILs. Each model was run with 50 random genotype replicates. Each replicate consisted of four Markov Chains with 4000 Metropolis steps. Sampling was performed using the software PyMC3 (SALVATIER *et al.* 2016). Model performance is measured using the Bayesian leave-one-out expected log pointwise predictive density (LOO-ELPD), quantifying the generalizability of the fitted model to validation data points. Higher LOO-ELPD indicate better model performance.

		RILs + RIAILs		**RILs**		**RIAILs**	
Index	**Model name**	LOO-ELPD	Δ Best	LOO-ELPD	Δ Best	LOO-ELPD	Δ Best
1	**Neutral**	-3501.2	-99.2	-2200.6	-33.4	-1493.1	-133.6
2	**Uniform**	-3478.2	-76.2	-2190.1	-22.9	-1472.6	-113.1

5	**Neutral + uniform**	-3422.2	-20.2	-2179.7	-12.6	-1365.1	-5.5
4	**Negative gamma**	-3422.2	-20.2	-2181.0	-13.8	-1360.3	-0.8
5	**3 effects**	-3403.1	-1.1	-2170.8	-3.7	-1360.4	-0.8
6	**Symmetric gamma**	-3402.0	**0**	-2168.2	-1.1	-1359.6	**0**
7	**Asymm. gamma**	-3402.3	-0.3	-2167.2	**0**	-1359.9	-0.3

(i) All lines (RILs + RIAILs = RI(AI)Ls). Reassuringly, the **neutral** model, in which mutational effects are constrained to equal 0, performs worst, with LOO-ELPD = -3501.2. The **uniform** effect model, in which mutational effects are constrained to be equal, is moderately better with LOO-ELPD = -3478.2. The posterior mean for the shared mutational effect (u) is negative and has a 95% credible interval not intersecting zero (u = -0.006; CI = -0.009, -0.005).

The next most complex model is the **neutral + uniform effect model**, in which mutations can either have a uniform non-zero effect with probability q or be neutral with probability $1- q$. This performed significantly better, with LOO-ELPD = -3422.2. Again, the mean mutational effect is inferred to be negative (u = -0.16, 95% CI = -0.24, -0.10), but with low probability (q = 0.064, 95% CI = 0.026, 0.114). The **negative Gamma** model, in which effects are constrained to be negative and sampled from a Gamma distribution, performs nearly identically to the neutral + fixed effect model, with LOO-ELPD = -3422.2.

371 All models summarized so far assume mutations must have a uniform sign. The first
372 model relaxing this assumption is the **3-effect model**, in which a mutation can be neutral with
373 probability $1 - q$, or have a fixed positive/negative effect with probabilities q^+ and q^- (in our
374 Bayesian model parametrization, $q^+ = q \times p^+$, $q^- = q \times (1 - p^+)$, where p^+ is the probability that a
375 mutation has a positive effect, given that it is non-neutral). This model showed a significant
376 improvement in performance with a LOO-ELPD = -3403.

377 Finally, the two-sided Gamma models (**symmetric** and **asymmetric Gamma**) provide a
378 moderate improvement over the 3-effect model. The two models have LOO-ELPD scores that
379 are nearly indistinguishable (symmetric gamma model = -3402, asymmetric gamma model = -
380 3402.3), indicating that the additional flexibility conferred by the asymmetric gamma model does
381 not confer higher generalizability to new data. For the asymmetric gamma model, the alpha
382 (scale) and beta (rate, inverse of the scale parameter) parameters for the positive and negative
383 halves of the distribution have nearly identical posterior distributions (**Supplemental Table 2**).
384 Additionally, the two-sided gamma models show very similar posterior distributions for all
385 parameters. We therefore focus our discussion on the more parsimonious symmetric gamma
386 model.

387 On average, mutations are slightly less likely to have a positive effect ($p^+ = 0.426$; 95%
388 CI = 0.294, 0.547). The posterior distribution of the effects of all 169 mutations shows that
389 39.6% of all mutations have a positive posterior mean effect (**Figure 2A**), consistent with the
390 posterior probabilities $p^+/^-$. However, individual mutations exhibit large credible intervals that
391 intersect zero (**Figure 3A**). The distribution of negative mean effects shows a longer tail than
392 the positive effects, but this asymmetry in shape was not reflected in the model selection results,
393 where the symmetric and asymmetric Gamma models have virtually identical performance. This

is likely a power issue, whereby the increased flexibility of the asymmetric Gamma model was not supported by enough data to result in likelihood improvements that can offset the penalty resulting from the higher model complexity.

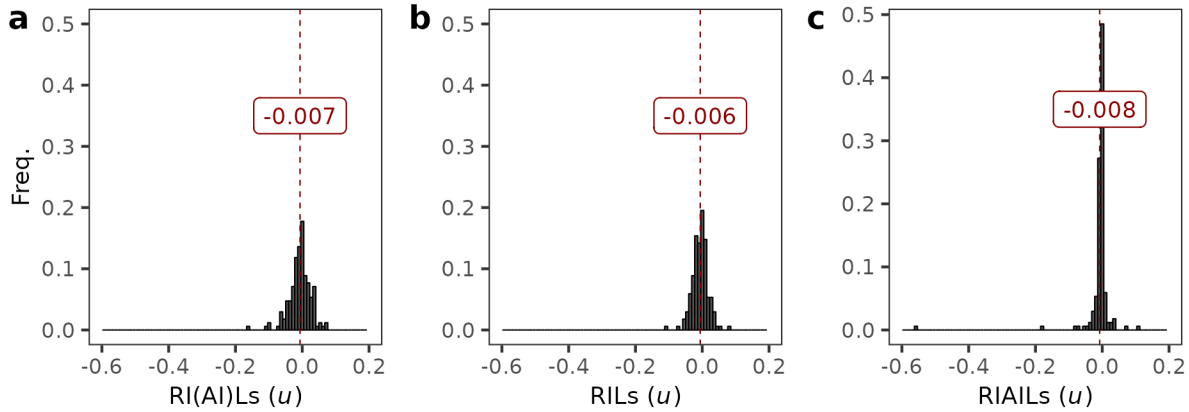

Figure 2 - Distribution of Bayesian posterior mutational effects on fitness. The distribution of mean mutational effects (u) calculated using the Bayesian MCMC method is shown. The distribution is calculated separately with (**a**) all lines (**b**), RILs only, or (**c**) RIAILs only. The vertical red line in each panel represents the mean of means for that population. The mean value for each panel is also annotated on the plots in red text.

(ii) RILs. The model selection results for the RILs are largely consistent with results based on the full set of RI(AI)Ls. The neutral and the fixed effect models have the lowest LOO-ELPD (**Table 1**). The two negative effects models have similar LOO-ELPD values and show significant improvement over the first two models. Finally, we see that the three two-sided models provide further substantial improvement over the one-sided model. The two-sided Gamma models produced very similar LOO-ELPD scores, while the 3-effect model has a moderately lower value. The distribution of mean mutational effects under the symmetric Gamma model are similar to results generated from the full set of RI(AI)Ls (Pearson's $r = 0.56$; **Figure 2B**).

(iii) RIAILs. Model selection results for the RIAILs reveal a different pattern. Although the neutral and fixed effect models still perform worst, performance of the models in which effects are constrained to be non-positive (in particular the negative Gamma model) is now close to that

of the two-sided models (**Table 1**). The similarity between the two-sided models and the negative-only model is supported by the change in the shape of the two-sided gamma models, in which the frequency of mutations with positive effects is lower ($q+ = 0.355$; 95% CI 0.119, 0.595). Inference from RIAILs resulted in an overall reduction in the mean posterior effects of mutations, such that the effects of most mutations are shrunk towards zero (**Figure 2C**). Additionally, the posterior variance of the mutational effects is lower in the RIAILs (mean posterior SD of mutational effects is 0.040, compared with 0.056 in the full set of RI(AI)Ls) (**Figure 3C**), even with the lower sample size. The mutational effects for the RIAILs are more weakly correlated to those inferred from the full set of RI(AI)Ls (Pearson's $r = 0.36$) than are the effects inferred from the RILs.

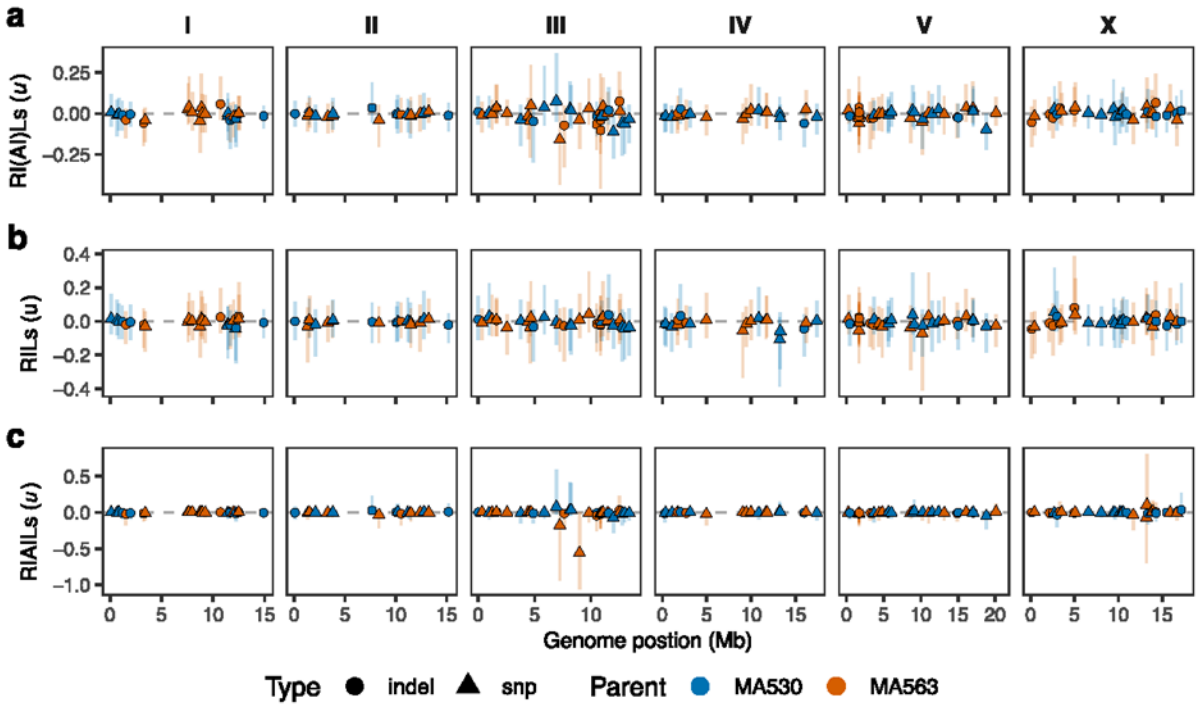

Figure 3 - Bayesian posterior mutational effects by genome position. The mutant loci are plotted by their physical position in the genome (x-axis) and their mean mutational effect (u) (y-axis), which was calculated using the Bayesian Markov chain Monte Carlo (MCMC) method. The colors indicate the parent of origin for the mutant locus (MA530-blue, MA563-orange) and the shapes show the mutant class (indel-circle, snp-triangle). The vertical lines plotted behind

each point represent the 95% confidence intervals of the mutant effect estimates. The mutational effects are calculated separately with all lines (**a**), RILs only (**b**), and RIAILs only (**c**).

(iv)The marginal DFE. The simplest way to infer the mutational effect at a locus is to calculate the mean value of all lines with a mutant allele and all lines with an ancestral allele at that locus; the difference is the marginal effect of the mutation at that locus. As a sanity check, we plotted the inferred Bayesian posterior effect against the marginal effect; ideally, the correlation should be +1. The correlations were positive, but well below 1 in all three cases (**Figure 4**). The magnitude of the marginal effects is typically much larger than that of the posterior effects. The difference is likely caused by LD, in that the marginal effect for a single mutation contains contributions from other linked mutations, which may inflate the estimates.

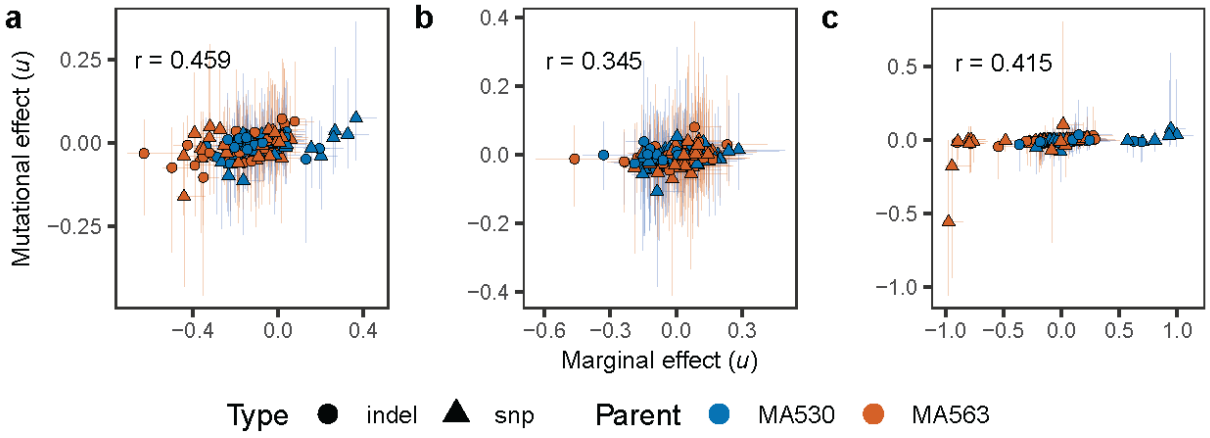

Figure 4 - The relationship between Bayesian posterior mutational effects and marginal effects. The effects are calculated separately using (**a**) all lines, (**b**) RILs only, or (**c**) RIAILs only. Each point represents a locus and is colored by the parent of origin (MA530-blue, MA563-orange). The shape of the point shows the mutant class (indel=circle, snp=triangle). 95% confidence intervals for the estimates are plotted as vertical and horizontal lines behind the points. Pearson's correlation coefficient (*r*) is displayed in the upper left of each panel.

Effects of mutant haplotypes

452 A major challenge is that many mutations are in high LD, making the effects of individual
453 mutations nearly unidentifiable (for example, if two mutations with effects, u_1 and u_2 are in
454 complete LD, we only have observations for the sum of their effect $u_1 + u_2$, making it impossible
455 to estimate u_1 and u_2 separately). To proceed, we first identified haplotype blocks consisting of
456 groups of loci in which LD among all pairs of consecutive loci $r^2 > 0.8$. We then designated two
457 haplotypes for each haplotype block. Among loci in a haplotype block, two types of haplotype
458 assignment can occur. Consider a haplotype block with two loci, each with an ancestral and a
459 mutant allele (coded 0 and 1). If the two loci are in positive LD, we have an ancestral haplotype
460 (00) and a double-mutant haplotype (11). If the two loci are in negative LD, we have two single-
461 mutant haplotypes, 01 and 10. Treating the data as haplotypes rather than individual loci reduces
462 the sample size from 169 (the number of loci) to 114 (the number of haplotypes). We restricted
463 this analysis to the symmetric Gamma model.

464 We acquired the posterior sample of a mutant haplotype by summing the posterior
465 samples of the individual mutations at each locus in the haplotype. We repeated this procedure
466 for the RILs, RIAILs and the full set of RI(AI)Ls. In all three cases, the distribution of the mean
467 mutant haplotype effects is skewed to the left (**Figure 5**). The percentage of mutant haplotypes

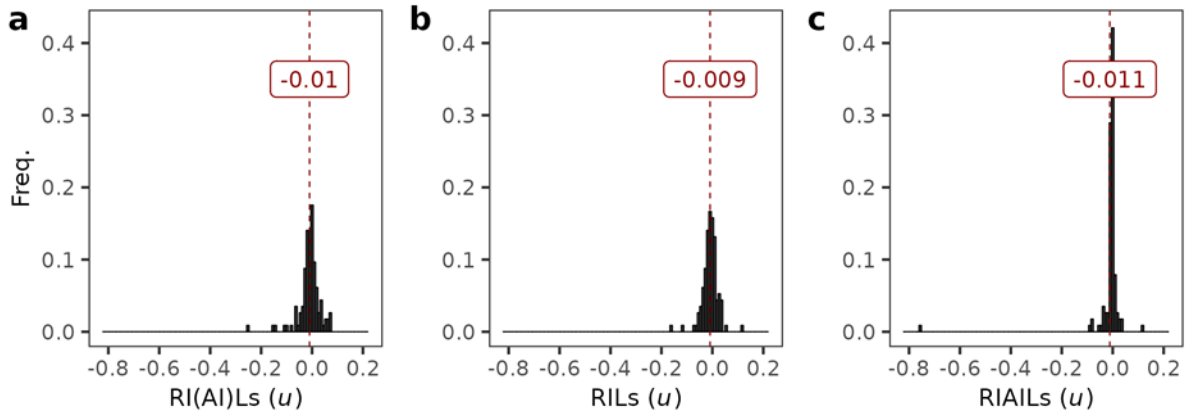

468

469 **Figure 5 - Distribution of Bayesian posterior mutant haplotype effects on fitness.** The
470 distribution of mean mutant haplotype effects (u) calculated using the Bayesian MCMC method

is shown. The distribution is calculated separately for (**a**) all lines, (**b**) RILs only, or (**c**) RIAILs. The vertical red line in each panel represents the mean of means for that population. The mean value for each panel is also annotated on the plots in red text.

with negative posterior means is 61.4% in the full set of RI(AI)Ls, 64.0% in the RILs, and 67.5% in the RIAILs. Again, inference from the RIAILs results in an overall reduction in the mean and variance of posterior effects of mutant haplotypes, relative to inferences from RILs and the full set of RI(AI)Ls. The mean absolute posterior mean effect for the negative mutant haplotypes based on RIAILs only (u^{-} = -0.022) is twice that of the positive mutant haplotypes (u^{+} = 0.011).

Finally, the lower LD in the RIAILs allowed us to identify a mutant haplotype with a strong negative effect located in a 6.05 Mb region between positions 3771123 and 9819058 on chromosome III (**Figure 6**). This haplotype contains 13 mutations, including 11 SNPs and 2 indels. The two mutant haplotypes are 1000111001100 for MA530, and 0111000110011 for

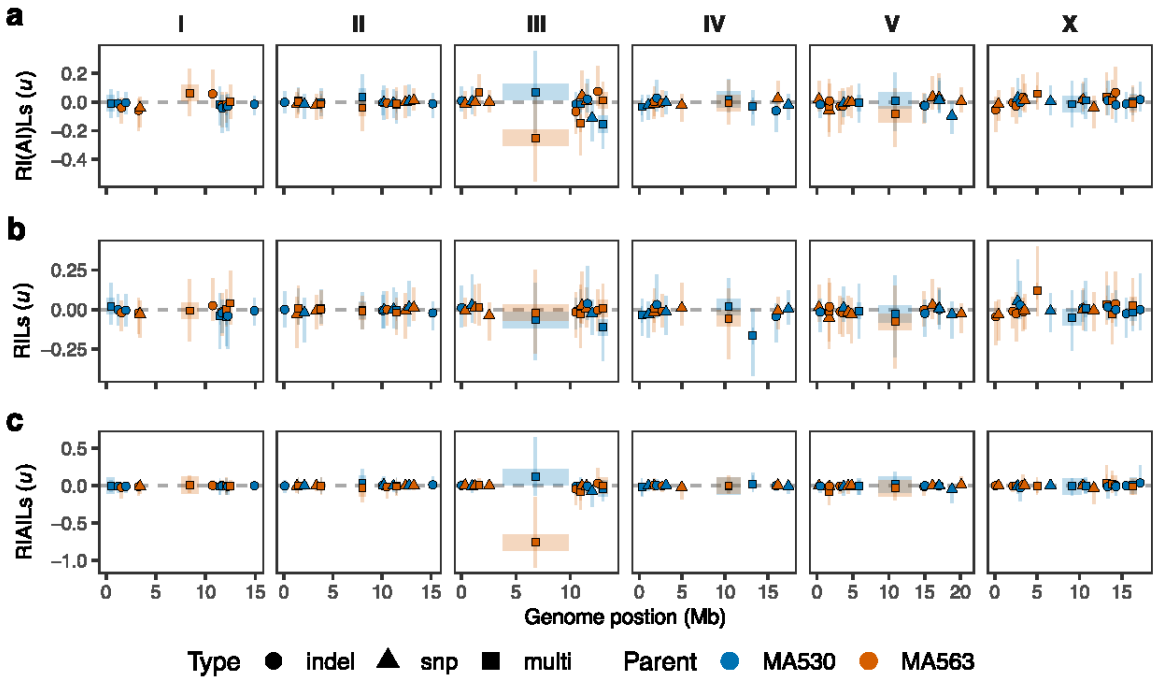

Figure 6 - Bayesian posterior mutant haplotype effects by genome position. The 114 mutant haplotypes are plotted by their physical position in the genome (x-axis) and their mean haplotype effect (u) (y-axis), which was calculated using the Bayesian Markov chain Monte Carlo (MCMC) method. The center of haplotypes are plotted as points and the genomic range of multi-locus haplotypes are represented by horizontal boxes plotted behind the points. The colors

490 indicate the parent of origin for the mutant haplotype (MA530-blue, MA563-orange). Multi-
491 locus mutant haplotypes are plotted with square points (multi), and the other single-locus
492 haplotypes are plotted with shapes based on mutation type (indel-circle, snp-triangle). The
493 vertical lines plotted behind each point represent the 95% confidence intervals of the haplotype
494 effect estimates. The haplotype effects are calculated separately with all lines (**a**), RILs only (**b**),
495 and RIAILs only (**c**).
496

497 MA563. The MA563 mutant haplotype has a large negative effect (u = -0.760; 95% CI -1.09, -
498 0.149), whereas the MA530 mutant haplotype shows a moderately strong positive mean effect (u
499 = 0.118; 95% CI -0.134, 0.647). However, their effects are strongly negatively correlated in the
500 posterior samples, i.e., if an estimated effect at the MA530 haplotype is large and negative, the
501 corresponding estimate at the MA563 haplotype is large and positive. The most we can say with
502 confidence is that the cumulative effect of mutations in this region is to reduce W by about 0.64
503 relative to the ancestor, which is sufficient to explain the decrease in fitness of MA563 relative to
504 the ancestor (**Supplemental Figure 5**).

505 The full list of mutations, along with parent of origin and their inferred effects, are
506 presented in **Supplemental Table 3**; fitness data are presented in **Supplemental Table 4**.
507

508 **DISCUSSION**

509 Unsurprisingly, mutations are deleterious, on average. Coincidentally or not, the point estimate
510 of the mean marginal effect on competitive fitness in the RI(AI)Ls, -0.0039, is extremely similar
511 to the same estimate from the full set of 80 MA lines of which the two parental lines were drawn.
512 Assuming that a random pair of MA lines differs by 160 mutations, the average mutational effect
513 estimated from the data of YEH *et al.* (2018, Table 1) is -0.0040. Given the substantial sources of
514 variation in these experiments, the concordance is remarkable. In a similar vein, YEH et al.
515 estimated the mutational heritability from the same data, $h_M^2 = V_L/2t$ = 0.00084/generation of

516 MA. Summed over the approximately 250 generations of MA, we predict a broad-sense
517 heritability $H^2 \approx 0.2$, about 2/3 of the observed value in this study. Or differently put, our
518 estimate of H^2 implies a mutational heritability $h_M^2 \approx 0.0012$. Given that both measures of
519 heritability are ratios of variances, the observed values are quite consistent.

520 Perhaps more surprising is the relatively high narrow-sense heritability of the mutational
521 effects (h^2=0.16), which explain roughly half of the heritable variance in fitness. There are no
522 comparable competitive fitness data from wild isolates, but ZHANG *et al.* (2021) estimated H^2
523 and h^2 for lifetime fecundity on solid media for a set of 121 *C. elegans* wild isolates. In their
524 assay h^2 (0.20) was about 1/3 of H^2 (0.63). In contrast to our RI(AI)Ls, which differ by about 85
525 mutations on average, the wild isolates differ by thousands of segregating variants. Comparison
526 of heritabilities is problematic because the upper bound is 1, which means that h^2 necessarily
527 reaches an asymptotic value. However, if we assume that the contribution of non-heritable
528 effects (V_E) is similar in the two studies – and we would naively expect that V_E is greater in a
529 competitive fitness assay than in a non-competitive assay because the competitor contributes to
530 V_E – the implication is that the asymptote is reached after at most a few hundred generations of
531 mutations have accumulated in the population.

532 The inclusion of both RILs and RIAILs in the experiment is fortuitous. If we only had
533 RILs to work with, we would have been much more confident in concluding that a large
534 proportion of mutations have positive effects. Ten generations of intercrossing in the RIAILs
535 broke up most of the initial LD, but not all of it, and it is clear that at least some of the apparently
536 greater fraction of positive-effect mutations in the RILs can be attributed to the confounding
537 effect of negative-effect mutations in LD. Inspection of the DFE along the chromosome (**Figure**

538 **3**) reveals a negative spatial autocorrelation: mutations inferred to have large positive effects are
539 usually in close proximity to one or more mutations with large negative effects.

540 This study was motivated by three antecedents: the studies of BÖNDEL *et al.* (2019), who
541 used a related crossing design to estimate the DFE from spontaneous MA lines in the unicellular
542 green alga *Chlamydomonas reinhardtii*; of GILBERT *et al.* (2021), who estimated the *C. elegans*
543 DFE from the standing site frequency spectrum among wild isolates; and those of VASSILIEVA *et*
544 *al.* (2000) and KEIGHTLEY *et al.* (2000), who estimated the DFE from the distribution of (non-
545 competitive) fitnesses among *C. elegans* MA lines. We consider each in turn.

546 BÖNDEL *et al*.'s crossing design differed from ours in a key way: they backcrossed MA
547 lines to the common ancestor rather than crossing two MA lines. Their design results in all
548 mutations being initially in complete coupling (positive) LD, rather than a random mix of
549 coupling and repulsion LD, as in our design. Nevertheless, their design is still constrained to
550 infer the cumulative effects of mutations in LD. They did not report LD, nor did they report the
551 distribution of mutational effects along the chromosomes (except as raw data). They too
552 observed a high proportion of mutations with positive effects on fitness; in their best-fit model
553 (two-sided Gamma with different means for positive and negative DFEs), the DFE was highly
554 leptokurtic, with posterior mean frequency of positive effects, q^+, of 84%. However, the
555 estimated mean (absolute) effect of deleterious mutations, u^-, was 4-5 times greater than the
556 mean positive effect, which reconciles the high frequency of mutations with positive effects with
557 the consistent and well-supported overall decline in fitness of the MA lines. They too observed a
558 strong positive correlation between the inferred posterior mean mutational effect at a locus and
559 the marginal effect, and that the Bayesian posterior DFE was shrunk toward zero compared to
560 the marginal effects.

561 GILBERT *et al*. used maximum likelihood, as implemented in the DFE-alpha software
562 (KEIGHTLEY and EYRE-WALKER 2007), to infer the DFE from segregating SNP variation in a set
563 of ~300 *C. elegans* wild isolates. They also analyzed data simulated under realistic parameters
564 of mutation and recombination to investigate the effect of self-fertilization on the inferred DFE.
565 They found that, while DFE-alpha reprises the input DFE quite faithfully when mating is
566 random, self-fertilization biases the results toward mutations of small negative effect, evidently
567 due to the slower decay of LD under selfing. Inclusion of a small fraction (0.1%) of beneficial
568 mutations similarly biases the inferred DFE of deleterious mutations toward small effects.
569 *C. elegans* MA lines invariably decline in fitness, and early studies concluded that the
570 mean deleterious mutational effect is quite large (~10-25 %) (ESTES *et al.* 2004; KEIGHTLEY and
571 CABALLERO 1997; VASSILIEVA *et al.* 2000), although none of those studies investigated
572 competitive fitness. The point estimate of the mean deleterious mutational effect from our
573 neutral + uniform effect model (Model 3) in the full set of RI(AI)Ls is -0.16 and the inferred
574 fraction of deleterious mutations (0.064) translates to a per-genome, per-generation deleterious
575 mutation rate of $U \approx 0.02$, very consistent with the aforementioned studies. Coincidentally or
576 not, our inference from RIAIL haplotypes that the *C. elegans* DFE consists of a very large
577 proportion of mutations with near-zero effects interspersed with a small number of mutations
578 with large negative effects is very similar to the conclusion of KEIGHTLEY *et al.* (2000), who
579 reached that conclusion from the distribution of fitnesses among *C. elegans* MA lines that had
580 been subjected to EMS mutagenesis.
581 Conclusions – Two primary conclusions emerge from this work. First, mathematics is no
582 substitute for recombination where inference of the DFE is concerned. When mutations are in
583 strong LD – repulsion or coupling – different combinations of positive and negative effects can

584 result in the same cumulative effect, possibly leading to the mistaken inference that the DFE
585 includes a large fraction of mutations with positive effects. However, posterior estimates at
586 linked loci will be strongly negatively correlated, which will not be true of unlinked loci. That
587 conclusion is obvious in hindsight, and should serve as a cautionary note. But second, the
588 unplanned inclusion in this study of RILs along with the RIAILs, and the large difference in
589 average LD between the two sets of lines, turns out to be informative. As LD is reduced in the
590 RIAILs vs. the RILs, the DFE becomes more leptokurtic, the inferred proportion of mutations
591 with negative effects increases, and the relative difference in magnitude between negative and
592 positive effects increases (negative effects become increasingly greater). When mutations are
593 binned into haplotypes, the most intuitive interpretation of the results is that almost all mutations
594 have effects that are very close to 0, and that the decline in fitness with MA is the result of a
595 small number of mutations with large negative effects – perhaps only one, on chromosome III in
596 the MA563 genome.

597 Looking ahead, we envision understanding of the DFE being advanced in three ways.
598 First, technical advances in high-throughput gene editing will allow efficient construction of
599 nearly-isogenic lines (NILs), removing the confounding effects of LD. The mutation spectrum
600 can be inferred, and a large random sample of spontaneous mutations can be engineered into a
601 common genomic background(s) and the DFE estimated as we have done here. Second, the DFE
602 of a common set of mutations should be estimated in a variety of contexts. We only assayed
603 fitness in one context in this experiment; it would be very interesting to see if, and how, the DFE
604 changes in different contexts. Finally, experimental estimates of the DFE can be employed as
605 strong priors in estimates of the DFE from standing polymorphism, which may have the added

606 benefit of facilitating estimates of demographic parameters by de-confounding selection from
607 demography.
608
609 **DATA AVAILABILITY STATEMENT**
610 Raw sequence data have been submitted to the NCBI BioProject database
611 (https://www.ncbi.nlm.nih.gov/bioproject/) under accession numbers PRJNA1083210
612 (RI(AI)Ls) and PRJNA429972 (parental MA lines). Cryopreserved stocks (G0 ancestor,
613 parental MA lines and RI(AI)Ls) are available upon request to CFB. All code for analyses is
614 available at https://github.com/Crombie-Lab/manuscript_DFE/tree/main
615
616 **ACKNOWLEGEMENTS**
617 We thank Joanna Dembek and Mike Snyder for expert work in the lab during the line
618 construction and assay phases of the experiment, and David McCandlish for comments on the
619 manuscript. Support was provided by NIH awards GM107227 to CFB, ECA, and JMP, and
620 GM127433 to CFB, ECA, and V. Katju.
621
622

LITERATURE CITED

AGARWAL, I., Z. L. FULLER, S. R. MYERS and M. PRZEWORSKI, 2023 Relating pathogenic loss-of-function mutations in humans to their evolutionary fitness costs. eLIFE **12**.

BAER, C. F., N. PHILLIPS, D. OSTROW, A. AVALOS, D. BLANTON *et al.*, 2006 Cumulative effects of spontaneous mutations for fitness in Caenorhabditis: Role of genotype, environment and stress. Genetics **174:** 1387-1395.

BAER, C. F., F. SHAW, C. STEDING, M. BAUMGARTNER, A. HAWKINS *et al.*, 2005 Comparative evolutionary genetics of spontaneous mutations affecting fitness in rhabditid nematodes. Proceedings of the National Academy of Sciences of the United States of America **102:** 5785-5790.

BÖNDEL, K. B., S. A. KRAEMER, T. SAMUELS, D. MCCLEAN, J. LACHAPELLE *et al.*, 2019 Inferring the distribution of fitness effects of spontaneous mutations in *Chlamydomonas reinhardtii*. PLoS Biology **17:** e3000192.

BOYKO, A. R., S. H. WILLIAMSON, A. R. INDAP, J. D. DEGENHARDT, R. D. HERNANDEZ *et al.*, 2008 Assessing the evolutionary impact of amino acid mutations in the human genome. Plos Genetics **4**.

BOYLE, E. A., Y. I. LI and J. K. PRITCHARD, 2017 An Expanded View of Complex Traits: From Polygenic to Omnigenic. Cell **169:** 1177-1186.

CANNATARO, V. L., S. A. MCKINLEY and C. M. S. ST. MARY, 2016 The implications of small stem cell niche sizes and the distribution of fitness effects of new mutations in aging and tumorigenesis. Evolutionary Applications **9:** 565-582.

CANNATARO, V. L., and J. P. TOWNSEND, 2018 Neutral Theory and the Somatic Evolution of Cancer. Molecular Biology and Evolution **35:** 1308-1315.

DAVIES, E. K., A. D. PETERS and P. D. KEIGHTLEY, 1999 High frequency of cryptic deleterious mutations in *Caenorhabditis elegans*. Science **285:** 1748-1751.

DURRETT, R., J. FOO, K. LEDER, J. MAYBERRY and F. MICHOR, 2010 Evolutionary dynamics of tumor progression with random fitness values. Theoretical Population Biology **78:** 54-66.

ESTES, S., P. C. PHILLIPS, D. R. DENVER, W. K. THOMAS and M. LYNCH, 2004 Mutation accumulation in populations of varying size: The distribution of mutational effects for fitness correlates in *Caenorhabditis elegans*. Genetics **166:** 1269-1279.

EYRE-WALKER, A., 2010 Genetic architecture of a complex trait and its implications for fitness and genome-wide association studies. Proceedings of the National Academy of Sciences of the United States of America **107:** 1752-1756.

FALCONER, D. S., 1989 *Quantitative Genetics*. Longman Scientific and Technical, Essex, UK.

FISHER, R. A., 1930 *The Genetical Theory of Natural Selection*. Clarendon Press, Oxford.

GILBERT, K. J., S. ZDRALJEVIC, D. E. COOK, A. D. CUTTER, E. C. ANDERSEN *et al.*, 2021 The distribution of mutational effects on fitness in *Caenorhabditis elegans* inferred from standing genetic variation. Genetics **220**.

HALLIGAN, D. L., and P. D. KEIGHTLEY, 2009 Spontaneous mutation accumulation studies in evolutionary genetics. Annual Review of Ecology Evolution and Systematics **40:** 151-172.

JAMES, J., C. KASTALLY, K. B. BUDDE, S. C. GONZÁLEZ-MARTÍNEZ, P. MILESI *et al.*, 2023 Between but not within species variation in the Distribution of Fitness Effects. Mol Biol Evol **13**.

JI, Y., Z. ZHOU, H. LIU and R. V. DAVULURI, 2021 DNABERT: pre-trained Bidirectional Encoder Representations from Transformers model for DNA-language in genome. Bioinformatics **37:** 2112-2120.

JOHRI, P., B. CHARLESWORTH and J. D. JENSEN, 2020 Toward an Evolutionarily Appropriate Null Model: Jointly Inferring Demography and Purifying Selection. Genetics **215:** 173-192.

KATJU, V., and U. BERGTHORSSON, 2019 Old Trade, New Tricks: Insights into the Spontaneous Mutation Process from the Partnering of Classical Mutation Accumulation Experiments with High-Throughput Genomic Approaches. Genome Biology and Evolution **11:** 136-165.

KEIGHTLEY, P. D., 1994 The distribution of mutation effects on viability in *Drosophila melanogaster*. Genetics **138:** 1315-1322.

KEIGHTLEY, P. D., and A. CABALLERO, 1997 Genomic mutation rates for lifetime reproductive output and lifespan in *Caenorhabditis elegans*. Proceedings of the National Academy of Sciences of the United States of America **94:** 3823-3827.

KEIGHTLEY, P. D., E. K. DAVIES, A. D. PETERS and R. G. SHAW, 2000 Properties of ethylmethane sulfonate-induced mutations affecting life-history traits in *Caenorhabditis elegans* and inferences about bivariate distributions of mutation effects. Genetics **156:** 143-154.

KEIGHTLEY, P. D., and A. EYRE-WALKER, 2007 Joint inference of the distribution of fitness effects of deleterious mutations and population demography based on nucleotide polymorphism frequencies. Genetics **177:** 2251-2261.

KEIGHTLEY, P. D., and A. EYRE-WALKER, 2010 What can we learn about the distribution of fitness effects of new mutations from DNA sequence data? Philosophical Transactions of the Royal Society B-Biological Sciences **365:** 1187-1193.

KIM, B. Y., C. D. HUBER and K. E. LOHMUELLER, 2017 Inference of the Distribution of Selection Coefficients for New Nonsynonymous Mutations Using Large Samples. Genetics **206:** 345-361.

KIM, D. U., J. HAYLES, D. KIM, V. WOOD, H. O. PARK *et al.*, 2010 Analysis of a genome-wide set of gene deletions in the fission yeast Schizosaccharomyces pombe. Nat Biotechnol **28:** 617-623.

KOUSATHANAS, A., and P. D. KEIGHTLEY, 2013 A comparison of models to Infer the distribution of fitness effects of new mutations. Genetics **193:** 1197-1208.

KRUGLYAK, L., A. BEYER, J. S. BLOOM, J. GROSSBACH, T. D. LIEBERMAN *et al.*, 2023 Insufficient evidence for non-neutrality of synonymous mutations. Nature **616:** E8-E9.

LATTER, B. D. H., and J. A. SVED, 1994 A Reevaluation of data from competitive tests shows high levels of heterosis in *Drosophila melanogaster*. Genetics **137:** 509-511.

LI, J. R., H. P. LI, M. JAKOBSSON, S. LI, P. SJÖDIN *et al.*, 2012 Joint analysis of demography and selection in population genetics: where do we stand and where could we go? Molecular Ecology **21:** 28-44.

LOEWE, L., and B. CHARLESWORTH, 2006 Inferring the distribution of mutational effects on fitness in Drosophila. Biology Letters **2:** 426-430.

MORROW, E. H., and T. CONNALLON, 2013 Implications of sex-specific selection for the genetic basis of disease. Evolutionary Applications **6:** 1208-1217.

MUKAI, T., 1964 Genetic structure of natural populations of *Drosophila melanogaster*. 1. Spontaneous mutation rate of polygenes controlling viability. Genetics **50:** 1-19.

ORR, H. A., 2000 The rate of adaptation in asexuals. Genetics **155:** 961-968.
PECK, J. R., G. BARREAU and S. C. HEATH, 1997 Imperfect genes, fisherian mutation and the evolution of sex. Genetics **145:** 1171-1199.
PURCELL, S., B. NEALE, K. TODD-BROWN, L. THOMAS, M. A. R. FERREIRA *et al.*, 2007 PLINK: A tool set for whole-genome association and population-based linkage analyses. American Journal of Human Genetics **81:** 559-575.
RAJAEI, M., A. S. SAXENA, L. M. JOHNSON, M. C. SNYDER, T. A. CROMBIE *et al.*, 2021 Mutability of mononucleotide repeats, not oxidative stress, explains the discrepancy between laboratory-accumulated mutations and the natural allele-frequency spectrum in *C. elegans*. Genome Research **31:** 1602-1613.
RAMANI, A. K., T. CHULUUNBAATAR, A. J. VERSTER, H. NA, V. VU *et al.*, 2012 The majority of animal genes are required for wild-type fitness. Cell **148:** 792-802.
RIVES, A., J. MEIER, T. SERCU, S. GOYAL, Z. LIN *et al.*, 2021 Biological structure and function emerge from scaling unsupervised learning to 250 million protein sequences. Proceedings of the National Academy of Sciences **118:** e2016239118.
ROCKMAN, M. V., and L. KRUGLYAK, 2008 Breeding designs for recombinant inbred advanced intercross lines. Genetics **179:** 1069-1078.
SALVATIER, J., T. V. WIECKI and C. FONNESBECK, 2016 Probabilistic programming in Python using PyMC3. PeerJ Computer Science **2:** e55.
SAXENA, A. S., M. P. SALOMON, C. MATSUBA, S. D. YEH and C. F. BAER, 2019 Evolution of the mutational process under relaxed selection in *Caenorhabditis elegans*. Molecular Biology and Evolution **36:** 239-251.
SCHULTZ, S. T., and M. LYNCH, 1997 Mutation and extinction: The role of variable mutational effects, synergistic epistasis, beneficial mutations, and degree of outcrossing. Evolution **51:** 1363-1371.
SHARON, E., S. A. A. CHEN, N. M. KHOSLA, J. D. SMITH, J. K. PRITCHARD *et al.*, 2018 Functional genetic variants revealed by massively parallel precise genome editing. Cell **175:** 544-557.
SHEN, X., S. SONG, C. LI and J. ZHANG, 2022 Synonymous mutations in representative yeast genes are mostly strongly non-neutral. Nature **606:** 725-731.
TATARU, P., M. MOLLION, S. GLEMIN and T. BATAILLON, 2017 Inference of Distribution of Fitness Effects and Proportion of Adaptive Substitutions from Polymorphism Data. Genetics **207:** 1103-1119.
TEOTÓNIO, H., D. MANOEL and P. C. PHILLIPS, 2006 Genetic variation for outcrossing among Caenorhabditis elegans isolates. Evolution **60:** 1300-1305.
THATCHER, J. W., J. M. SHAW and W. J. DICKINSON, 1998 Marginal fitness contributions of nonessential genes in yeast. Proceedings of the National Academy of Sciences of the United States of America **95:** 253-257.
VASSILIEVA, L. L., A. M. HOOK and M. LYNCH, 2000 The fitness effects of spontaneous mutations in *Caenorhabditis elegans*. Evolution **54:** 1234-1246.
VEHTARI, A., A. GELMAN and J. GABRY, 2017 Practical Bayesian model evaluation using leave-one-out cross-validation and WAIC. Statistics and Computing **27:** 1413-1432.
VEHTARI, A., A. GELMAN, D. SIMPSON, B. CARPENTER and P.-C. BÜRKNER, 2021 Rank-Normalization, Folding, and Localization: An Improved $\widehat{R}$ for Assessing Convergence of MCMC (with Discussion). Bayesian Analysis **16:** 667-718, 652.
WICKHAM, H., 2009 *ggplot2*. Springer, New York, NY.

YEH, S.-D., A. S. SAXENA, T. A. CROMBIE, D. FEISTEL, L. M. JOHNSON *et al.*, 2018 The mutational decay of male-male and hermaphrodite-hermaphrodite competitive fitness in the androdioecious nematode *C. elegans*. Heredity **120:** 1-12.

ZHANG, G., J. D. MOSTAD and E. C. ANDERSEN, 2021 Natural variation in fecundity is correlated with species-wide levels of divergence in *Caenorhabditis elegans*. G3 Genes|Genomes|Genetics **11**.

ZHANG, X. S., J. L. WANG and W. G. HILL, 2004 Influence of dominance, leptokurtosis and pleiotropy of deleterious mutations on quantitative genetic variation at mutation-selection balance. Genetics **166:** 597-610.

772 **Figure Legends**

773

774 **Figure 1 - Intrachromosomal pairwise linkage disequilibrium (LD).** (**a**) Pairwise LD (r^2)
775 calculated with all lines (RIAILs + RILs), (**b**) RILs only, and (**c**) RIAILs only. Each heat map
776 represents a chromosome with pairwise LD (r^2) between mutant loci colored as shown in the
777 legend. The colored lines above each chromosome represent the parental origin of the mutant
778 allele (MA530-solid blue, MA563-dashed orange). These lines also show the relative physical
779 position of mutant loci across each chromosome; the far-left vertical line represents the first
780 mutant locus on the chromosome and the far-right vertical line represents the last mutant locus.

781

782 **Figure 2 - Distribution of Bayesian posterior mutational effects on fitness.** The distribution
783 of mean mutational effects (*u*) calculated using the Bayesian MCMC method is shown. The
784 distribution is calculated separately with (**a**) all lines (**b**), RILs only, or (**c**) RIAILs only. The
785 vertical red line in each panel represents the mean of means for that population. The mean value
786 for each panel is also annotated on the plots in red text.

787

788 **Figure 3 - Bayesian posterior mutational effects by genome position.** The mutant loci are
789 plotted by their physical position in the genome (x-axis) and their mean mutational effect (u) (y-
790 axis), which was calculated using the Bayesian Markov chain Monte Carlo (MCMC) method.
791 The colors indicate the parent of origin for the mutant locus (MA530-blue, MA563-orange) and
792 the shapes show the mutant class (indel-circle, snp-triangle). The vertical lines plotted behind
793 each point represent the 95% confidence intervals of the mutant effect estimates. The mutational
794 effects are calculated separately with (**a**) all lines, (**b**) RILs only, and (**c**) RIAILs only.

Figure 4 - The relationship between Bayesian posterior mutational effects and marginal effects. The effects are calculated separately using (**a**) all lines, (**b**) RILs only, or (**c**) RIAILs only. Each point represents a locus and is colored by the parent of origin (MA530-blue, MA563-orange). The shape of the point shows the mutant class (indel=circle, snp=triangle). 95% confidence intervals for the estimates are plotted as vertical and horizontal lines behind the points. Pearson's correlation coefficient (*r*) is displayed in the upper left of each panel.

Figure 5 - Distribution of Bayesian posterior mutant haplotype effects on fitness. The distribution of mean mutant haplotype effects (u) calculated using the Bayesian MCMC method is shown. The distribution is calculated separately for (**a**) all lines, (**b**) RILs only, or (**c**) RIAILs. The vertical red line in each panel represents the mean of means for that population. The mean value for each panel is also annotated on the plots in red text.

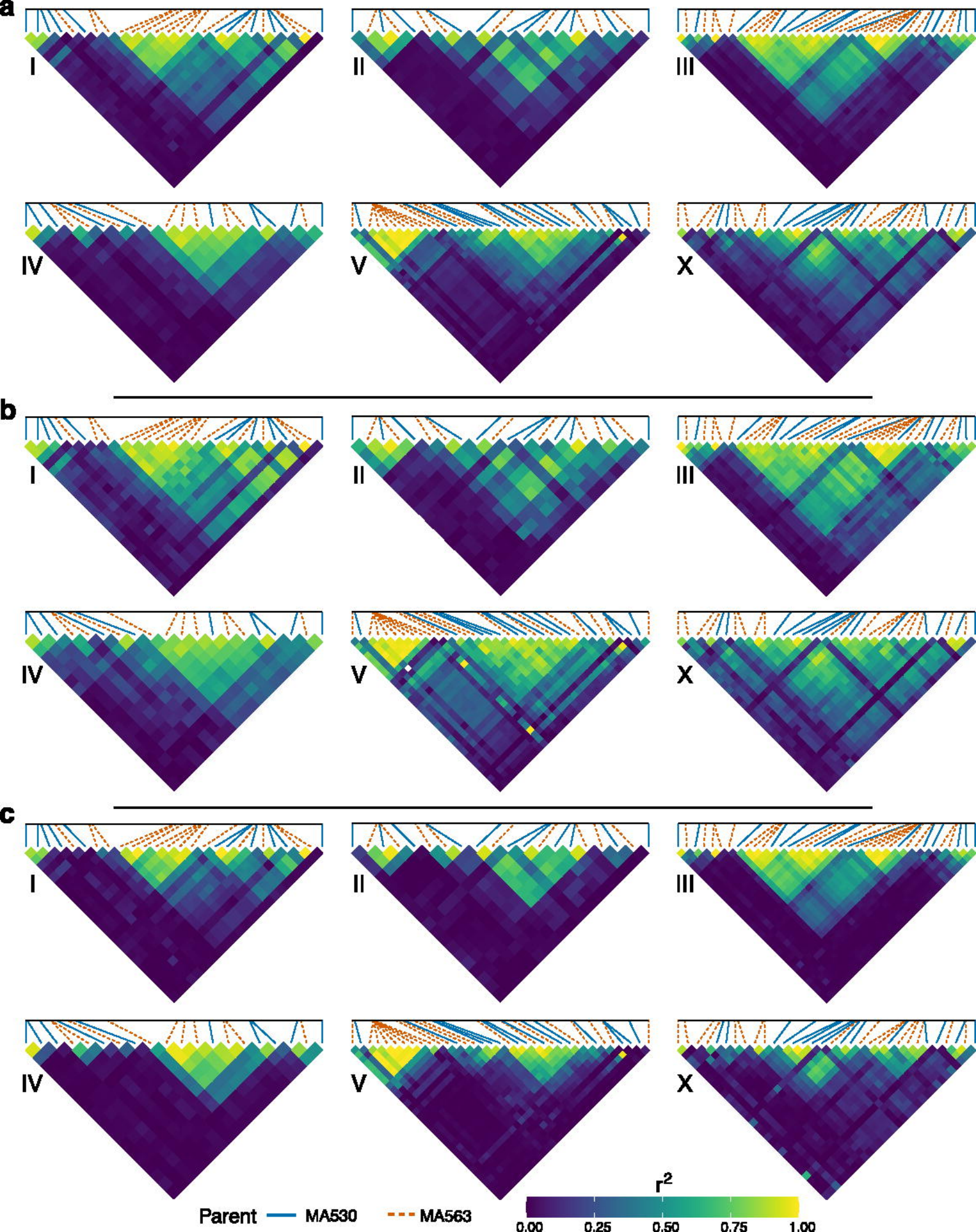
a
I
II
III
IV
V
X
b
I
II
III
IV
V
X
c
I
II
III
IV
V
X
Parent
MA530
MA563
r2
0.00
0.25
0.50
0.75
1.00

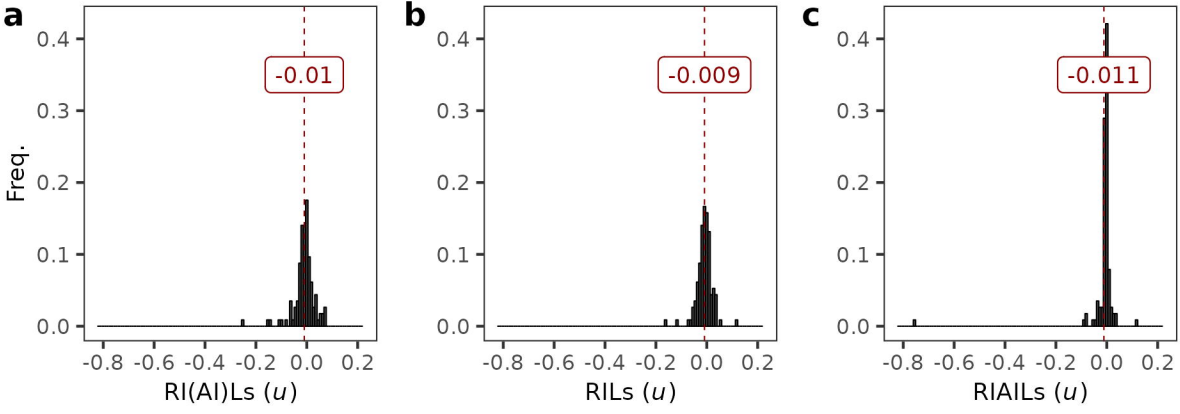
a
b
c
Freq.
0.0
0.1
0.2
0.3
0.4
-0.01
-0.009
-0.011
-0.8 -0.6 -0.4 -0.2 0.0 0.2
RI(AI)Ls (u)
RILs (u)
RIAILs (u)

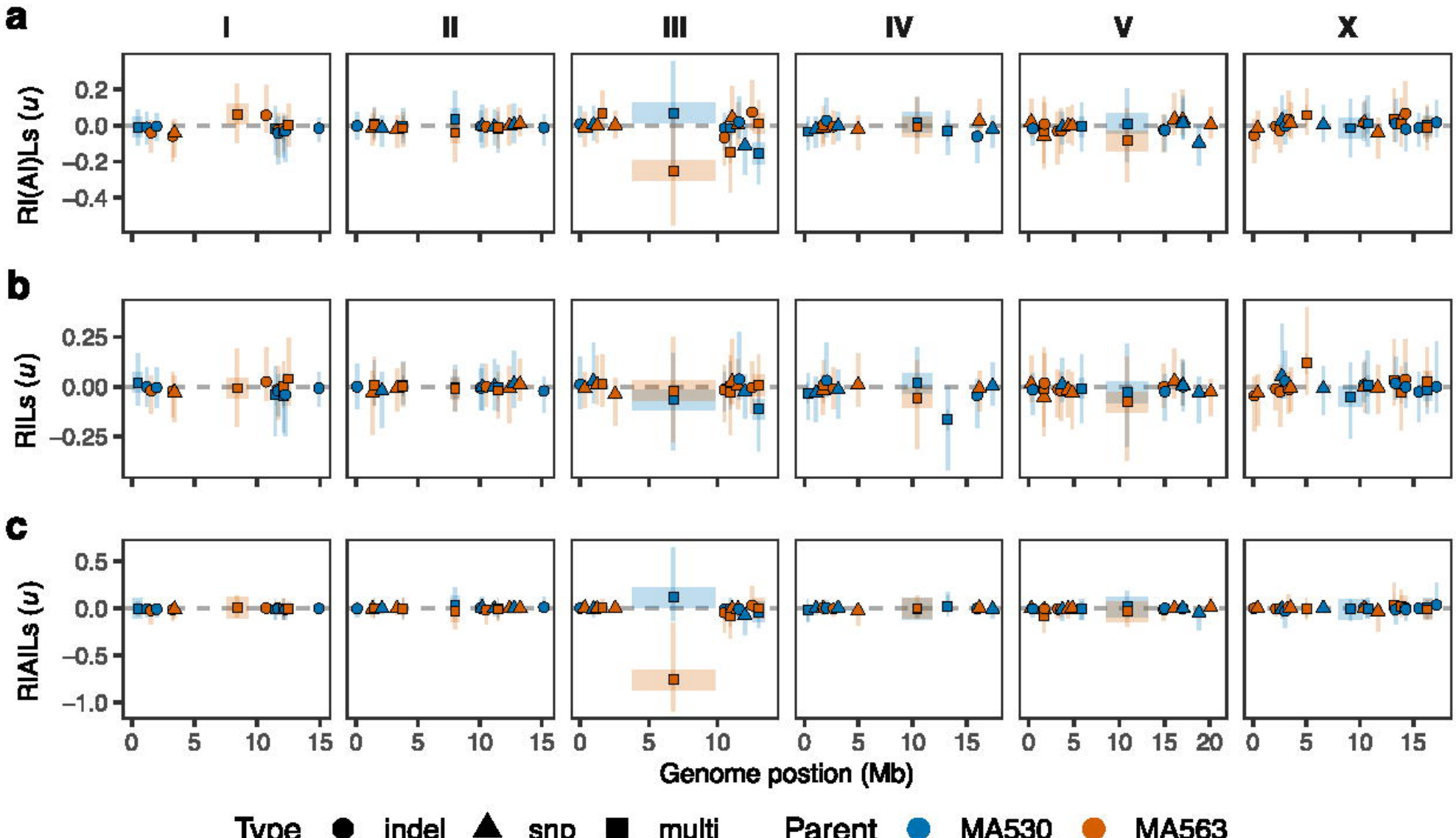
a
I
II
III
IV
V
X
RI(AI)Ls (u)
0.2
0.0
−0.2
−0.4
b
RILs (u)
0.25
0.00
−0.25
c
RIAILs (u)
0.5
0.0
−0.5
−1.0
0
5
10
15
20
Genome postion (Mb)
Type
indel
snp
multi
Parent
MA530
MA563

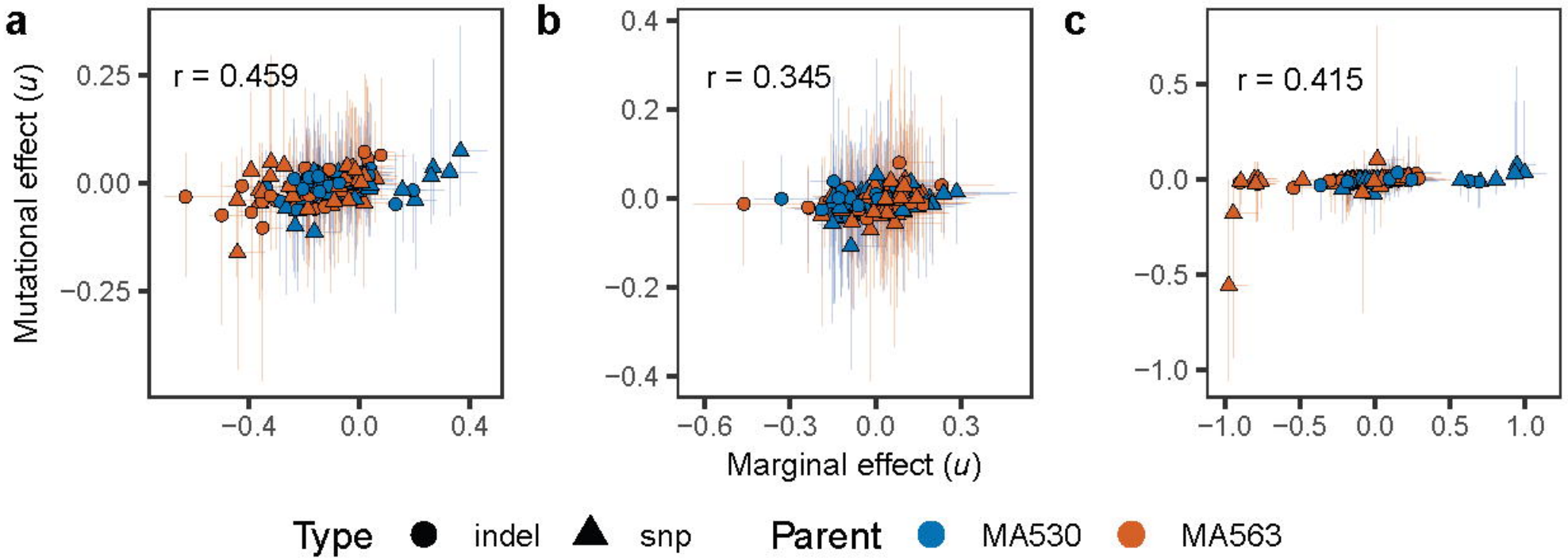
a
b
c
r = 0.459
r = 0.345
r = 0.415
Mutational effect (u)
Marginal effect (u)
0.25
0.00
−0.25
−0.4
0.0
0.4
0.4
0.2
0.0
−0.2
−0.4
−0.6
−0.3
0.0
0.3
0.5
0.0
−0.5
−1.0
−1.0
−0.5
0.0
0.5
1.0
Type
indel
snp
Parent
MA530
MA563

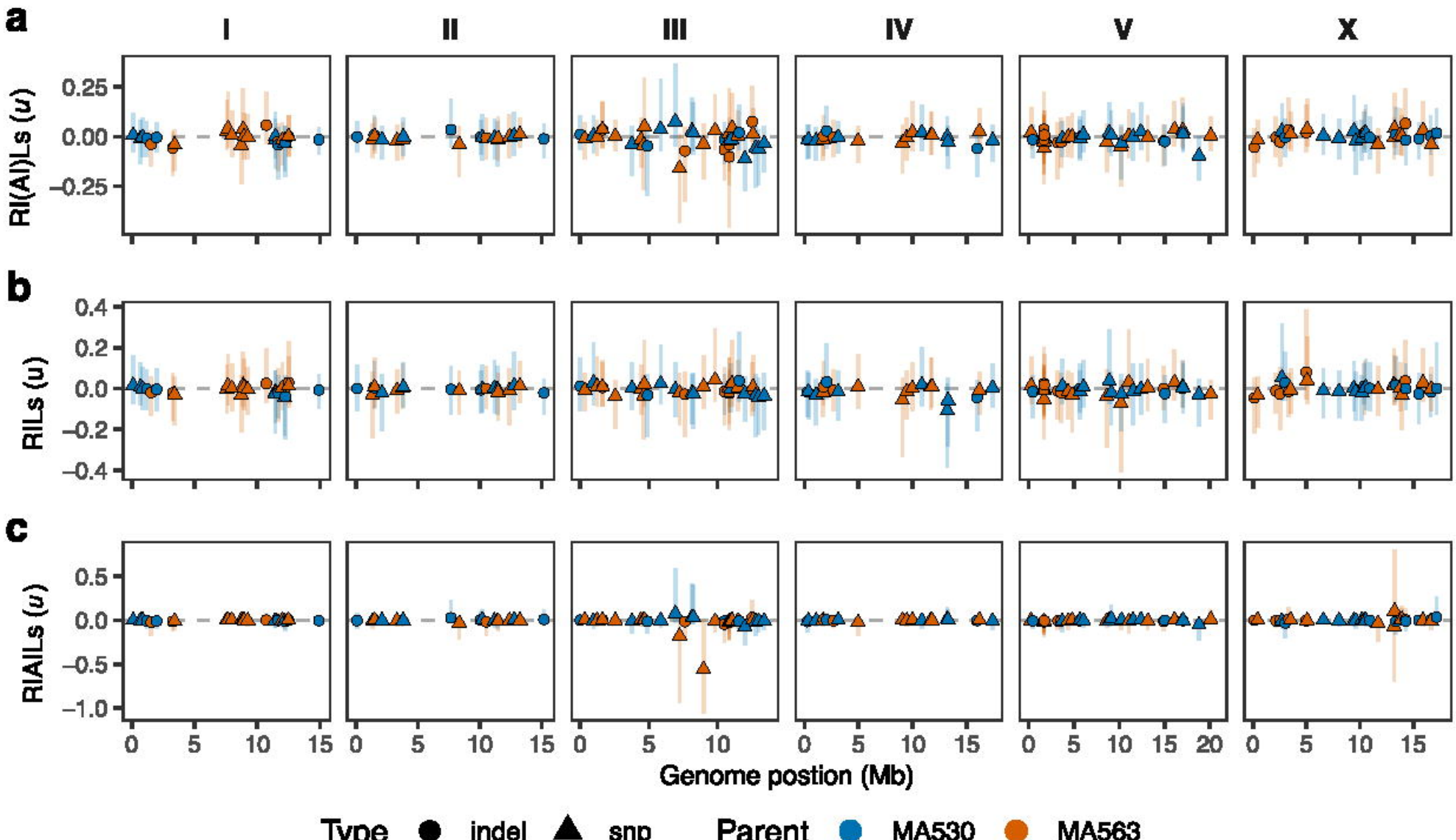
a
I
II
III
IV
V
X
RI(AI)Ls (u)
0.25
0.00
−0.25
b
RILs (u)
0.4
0.2
0.0
−0.2
−0.4
c
RIAILs (u)
0.5
0.0
−0.5
−1.0
0
5
10
15
20
Genome postion (Mb)
Type
indel
snp
Parent
MA530
MA563

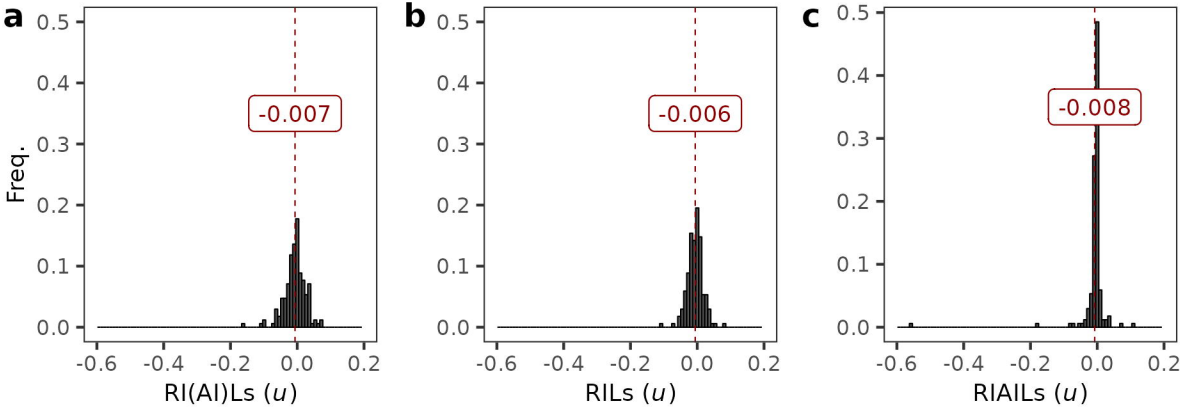
a
b
c
Freq.
0.5
0.4
0.3
0.2
0.1
0.0
-0.007
-0.006
-0.008
-0.6
-0.4
-0.2
0.0
0.2
RI(AI)Ls (u)
RILs (u)
RIAILs (u)